CHAPTER 1

INTRODUCTION AND LITERATURE REVIEW


1.1 HISTORICAL DEVELOPMENT OF TITANIUM AND ITS ALLOYS

Titanium was first recognized in 1791 in the iron sand ($FeO.TiO_2$) by William Gregor, an English clergyman, and an amateur mineralogist. After that similar observation was made in 1795 by a German chemist, Martin Klaproth who analyzed a mineral rutile (TiO_2) and he named the element titanium after the Titans, the powerful sons of the earth in Greek mythological [Polmer (2006)]. Titanium is the fourth gorgeous metal after aluminum, iron, and magnesium. Extraction of titanium from its ores was not developed on a commercial scale until the Kroll's process was developed in 1950. Today, a large number of titanium and titanium alloys are used in various applications like chemical and petrochemical industries as well as other consumer goods such as cameras, watches, and sports equipments. Titanium alloys are widely used in aerospace engine at different temperatures as shown in Fig. 1.1. However, one of the largest users of titanium is still the aerospace industry, where titanium alloys are used as material in compressor discs and blades in jet engines and airframe structures in aircraft, space rockets, and satellites [Lin et al. (2011), Marmy et al. (2000)].

The most popular titanium alloy Ti–6Al–4V was the first high-temperature titanium alloy developed in 1954s in the United States [Leyans et al. (2003)]. It is an important α+β titanium alloy known as workhorse alloy because of its approximately 60% use in comparison of all titanium alloy products. It has low density, high specific strength (strength/density), and good corrosion resistance and is used for a wide range of applications [Leyans et al. (2003), Li et al. (2010)]. This alloy has been developed for

high-temperature applications with superior mechanical strength, corrosion resistance and fatigue resistance at elevated temperature [Boyer (1996)]. It is also used in medical applications for implanting in human body especially as dental implants and knee joints due to its excellent biocompatibility, good corrosion resistance, and mechanical properties [Jun et al. (2010), Wen et al. (2004)]. Corrosion resistance of this alloy is due to a thin protective layer of TiO_2 (rutile) which protects it from marine atmosphere as well as chemicals [Gurappa (2003), Wen et al. (2007)].
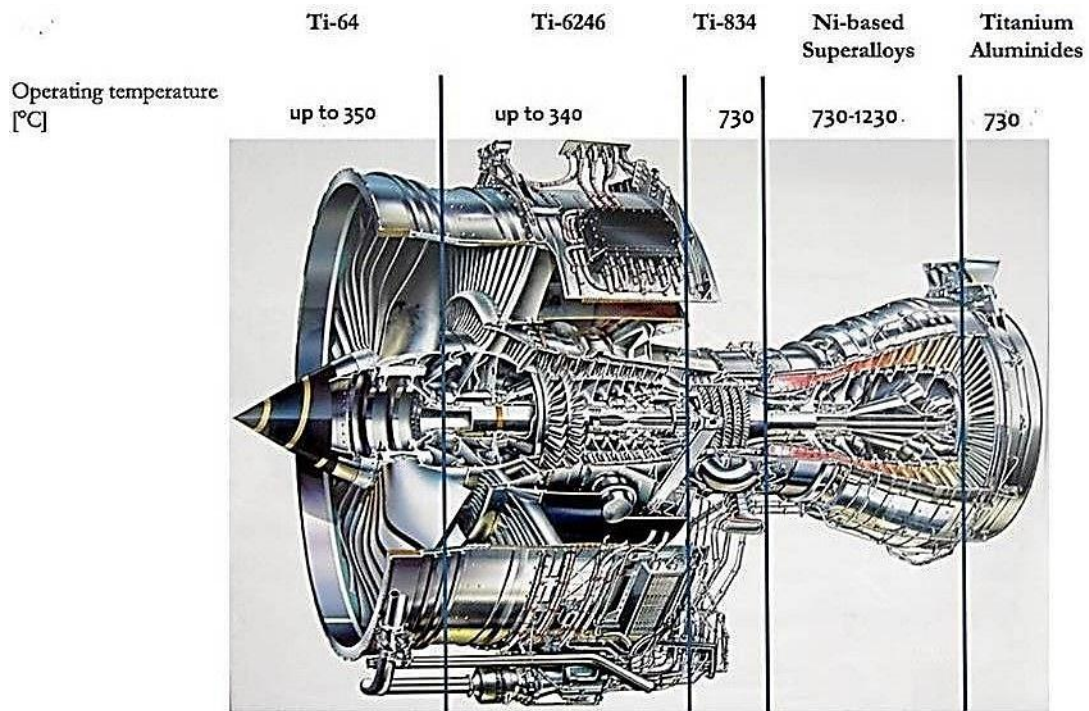
Fig. 1.1 Sectional view of one model of the Rolls Royce RB 211 gas turbine engine [courtesy: www.thomassourmail.net/turbine.html].

However, among titanium and its alloy series, commercially pure titanium (cp-Ti) is the second most used for application in the aerospace, chemical industries, and medical devices. Titanium alloys have higher specific strength at elevated temperature

than that of aluminum and steel (Fig. 1.2). However, titanium is 40% lighter than steel and 60% heavier in comparison of aluminum.
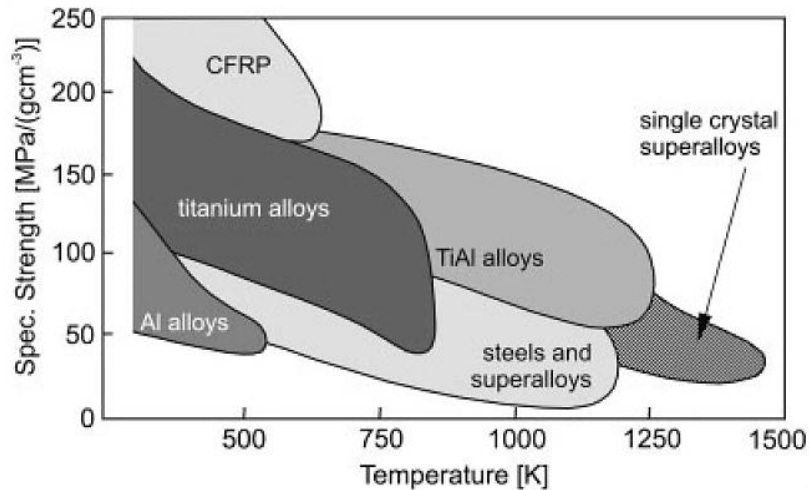
Fig. 1.2 Specific strength vs temperature of selected structural materials compared with titanium alloys [Leyans et al. (2003)].

1.2 CRYSTAL STRUCTURE AND PHASE STABILITY OF TITANIUM AND ITS ALLOYS

Titanium undergoes an allotropic transformation from the low temperature α (HCP) phase to the high temperature β (BCC) phase at 882±2 °C. Figure 1.3 shows α to β phase transformation. The temperature at which β to α transformation occurs is called the β-transus and depends on the amount and type of alloying elements added. The alloying elements that are dissolved in titanium may stabilize α or β phase. Titanium and its alloys react with interstitial elements such as oxygen, nitrogen, and hydrogen, below their respective melting points. In its reactions with other elements, titanium may form solid solutions and compounds with metallic, covalent or ionic bonding. Major alloying elements, added to improve mechanical properties and corrosion resistance, are classified as α-stabilizer, or β-stabilizers.
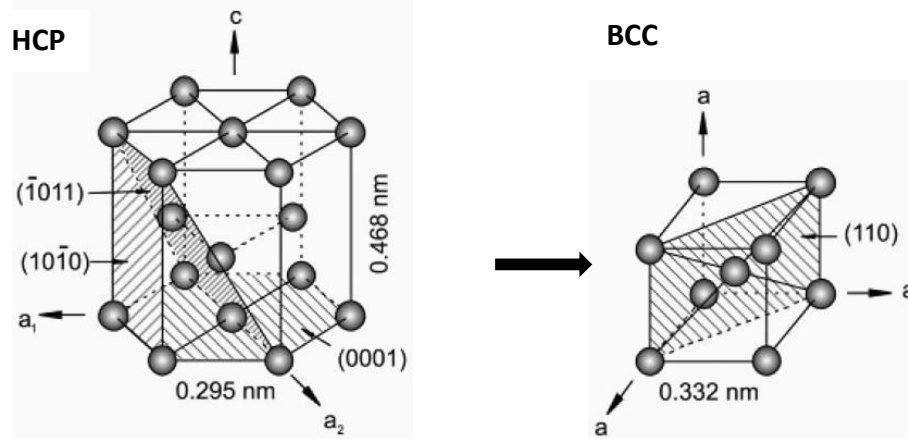
Fig. 1.3 Crystal structure of α (HCP) and β (BCC) phase [Leyans et al. (2003)].

The alloying elements are generally classified into three categories as α-stabilizer, β-stabilizer and neutral. The α-stabilizing elements extend the α phase field to higher temperatures, while β-stabilizing elements shift the β phase field to lower temperatures. Neutral elements have only minor influence on the β transus temperature.

1.2.1 *Alpha (α) Stabilizers*

The main α-stabilizing elements are Al, Sn, O and N which improve the solid solution strengthening and corrosion resistance. Al is the principle alloying element because it is one of the strongest α stabilizers. Al is a very effective alpha-strengthening element at ambient and elevated temperatures up to about 550 °C. The low density of aluminum is an additional advantageous feature but the amount that can be added is limited because of the formation of a brittle titanium aluminium compound, Ti_3Al, at aluminum contents exceeding about 8wt. %. Sn also plays the role of α phase stabilizer to improve ductility [Singh et al. (2002)]. Oxygen and nitrogen are normally present as impurities and contribute to interstitial hardening. A small amount of oxygen is used to provide a specific range of strength levels in several grades. These alloying elements

tend to increase the strength but decrease the ductility of Ti alloys [Polmer (2006), Leyans et al. (2003)].

1.2.2   Beta (β) Stabilizers

Those elements which reduce the transformation temperature (α/β), strengthen the beta phase and exhibit low alpha phase solubility are known as β-stabilizers. They are of two types; β isomorphous elements, and β eutectoid elements. β isomorphous elements used in titanium alloys are Ta, V, Mo, and Nb. They have complete solid solubility in β titanium. Sufficient concentrations of these elements make it possible to stabilize the β phase to room temperature [Polmer (2006)]. On the other hand, the β eutectoid stabilizers which are generally used for alloying with Ti are Cr, Fe, and Si while Ni, Cu, Mn, W, Pd, and Bi have only limited usage [Polmer (2006), Leyans et al. (2003)].

1.2.3   Neutral Elements

Zr and Hf are considered neutral elements because they lower the α/β transformation temperature only slightly and then increase the transformation temperature again at higher concentrations. Zr and Hf both exhibit the same β to α allotropic phase transformation and are isomorphous with both the phases of titanium. Sn has little influence on the α/β phase boundary.

1.3   CLASSIFICATION OF TITANIUM ALLOYS

Based on the phases present at room temperature, titanium alloys are classified into four different groups of α alloys (commercially pure titanium), near α alloys, β alloys, and α+β alloys. Figure 1.4 shows schematically the three-dimensional phase diagram, which is composed of two phase diagrams with α and β stabilizing elements

respectively. According to this diagram, α alloys comprise of α phase and are exclusively alloyed with α stabilizing elements. If little quantity of β stabilizing elements is added, they are referred to as near α alloy. The α+β alloys are the most widely used titanium alloys [Evans (1998)]. These alloys have β volume fraction ranging from about 5 to 40% at room temperature. If the percentage of β-stabilizing elements is further increased to a level where β no longer transforms to martensite upon fast quenching, the alloys are still in the two-phase field and the metastable class of β alloys is reached. It should be noted that these alloys can still reveal an equilibrium volume fraction of more than 50% of β. Finally, the single-phase β alloys mark the end of the alloying scale of the conventional titanium alloys [Leyans et al. (2003)].
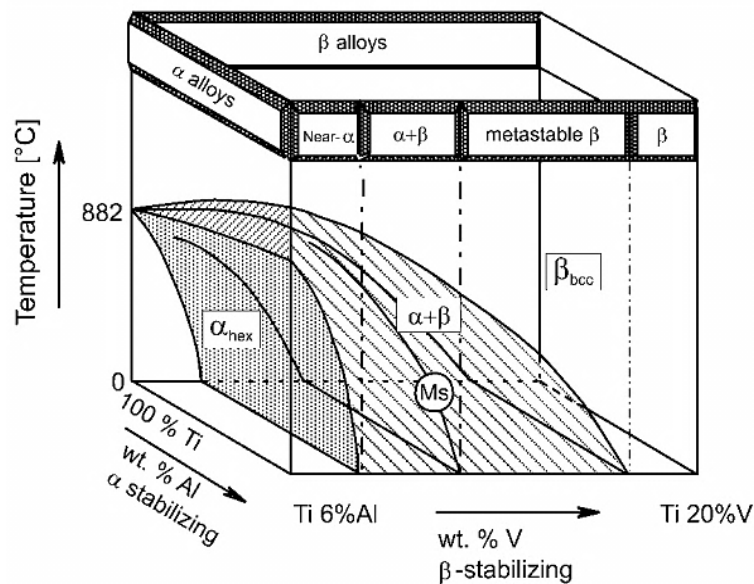
Fig. 1.4 Schematic three-dimensional phase diagram to classify titanium alloys [Leyans et al. (2003)].

1.3.1   Commercially Pure Titanium (α-alloys)

Alpha is the low-temperature allotrope of titanium, and the microstructure of α alloys consists predominantly of the α-phase. They are used as airframes, heat

exchangers due to their good creep resistance and corrosion resistance. They are also used in medical devices because of their corrosion resistance. α alloys are the most weldable and non-heat treatable titanium alloys. They are also used largely in cryogenic applications at -253 °C. Their properties are strongly dependent on texture [Polmer (2006)]. The typical applications and tensile strength of α alloys are recorded in Table 1.1.
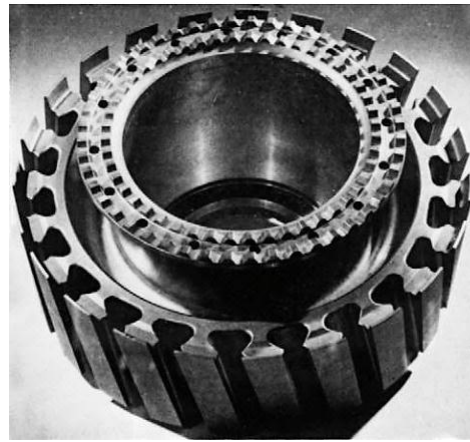
Table 1.1 Typical applications and tensile strength of different grades of α alloys [Polmer (2006), Leyans et al. (2003)].

S. No.	Grade	wt.% Ti	Applications	Tensile strength	
				YS (MPa)	UTS (MPa)
1.	High purity	99.98	airframes, heat exchangers and medical device	140	235
2.	1	99.5	airframes, heat exchangers and marine chemical parts	170-310	>240
3.	2	99.2	airframes, heat exchangers and marine chemical parts	>310	390-540
4.	3	99.1	airframes, aircraft engine, medical and chemical parts	350-450	550-600
5.	4	99.0	airframes, aircraft engine and chemical parts	480-655	>550

1.3.2 *Near–α Alloys*

Near–α alloys contain a small amount of β stabilizers like Mo and V which provide a microstructure of β phase dispersed in the α phase structure. They are used in aircraft gas turbine engine components like compressor disc at high temperatures up to 550°C. A compressor disc made of near–α alloy Ti–6Al–5Zr–0.5Mo–0.25Si (IMI 685) is shown in Fig. 1.5. The presence of the β phase permits two-phase strengthening

through control over the scale, morphology and distribution of the two phases. The mechanical properties of near α alloys are superior to those of α-alloys, further, due to the presence of β phase, these alloys are heat treatable. They possess higher strength than those of α alloys at room-temperature and also show good creep resistance at temperature up to 600 °C. The typical applications and tensile strength of some near-α alloys are recorded in Table 1.2.

**Fig. 1.5** Forged compressor disc made of the near α alloy IMI 685 [Polmer (2006)].

Table 1.2 Typical applications and tensile strength of the near-α alloys [Polmer (2006), Leyans et al. (2003)].

S. No.	Alloy	Applications	Tensile strength	
			YS (MPa)	UTS (MPa)
1.	Ti–6Al–5Zr–0.5Mo–0.25Si	jet engine parts, gas turbine compressor disc	850-910	990-1020
2.	Ti–11Sn–2.25Al–5Zr–1Mo–0.2Si	gas turbine compressor disc	990	1100
3.	Ti–5.5Al–3.5Sn–3Zr–1Nb–0.25Mo–0.3Si	jet engine parts	860	960
4.	Ti–5.8Al–4Sn–3.5Zr–0.7Nb–0.5Mo–0.35Si	gas turbine components	890-910	1000-1035

1.3.3   *β Alloys*

β alloys are used in aerospace industries due to their high strength, good fatigue resistance, and corrosion resistance [Niinomi (1998)]. They contain substantial amount of β phase stabilizers, preventing β to α transformation at high cooling rates of quenching. There are two types of β alloys: metastable and stable. They contain sufficient alloying elements that enable the β phase to be retained in either metastable or in stable condition after cooling to room temperature during heat treatment, as shown in Fig. 1.6.
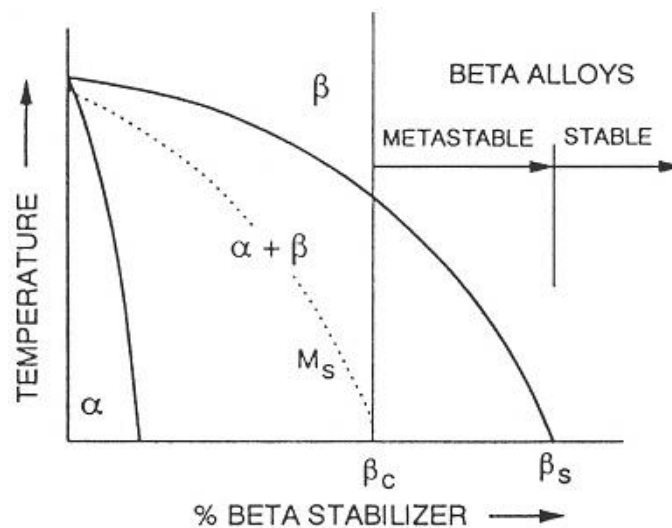
Fig. 1.6 Pseudo-binary β isomorphous phase diagram showing locations of metastable and stable β titanium alloys [Leyans et al. (2003)].

The alloys with compositions between the point of intersections of the Ms and β transus line (βs) at room temperature axis are commonly referred to as metastable β titanium alloys (Fig 1.6). More highly alloyed compositions to the right of βs are considered to be stable β alloys. On quenching, instead of forming martensite, β alloys form the metastable β phase due to the presence of sufficient amount of beta stabilizers.

They can achieve very high strengths and are the most easily mechanically formed titanium alloys due to their BCC crystal structure. However, they have relatively high density [Boyer (1996)]. The typical applications and tensile strength of β alloy are recorded in Table 1.3.

Table 1.3 Typical applications and tensile strength of the β alloys [Polmer (2006), Leyans et al. (2003)].

S. No.	Alloy	Applications	Tensile strength	
			YS (MPa)	UTS (MPa)
1.	Ti–11.5Mo–6Zr–4.5Sn	aircraft fasteners, rivets, orthodontic devices	800-1200	900-1300
2.	Ti–15V–3Cr–3Al–3Sn	airframe sheet, tubing and fasteners	800-1000	800-1100
3.	Ti–3Al–8V–6Cr–4Mo–4Zr	aircraft fasteners, tubular casings for oil, gas	800-1200	900-1300
4.	Ti–10V–2Fe–3Al	airframes, landing gear, bar and plate.	1000-1200	1000-1400

1.3.4   *α+β Alloys*

α+β alloys contain α phase stabilizing elements with 4-6% of β stabilizing elements and have α+β microstructure, with primary α (HCP) and retained β (BCC) phase. In the group of α+β alloys, Ti–6Al–4V alloy is the most popular titanium alloy. More than 50% of all the alloys in use today are of this composition [Boyer, (1996)]. Desired microstructure and properties are obtained through annealing, quenching and tempering. Fig. 1.7 shows ternary phase diagram of Ti–6Al–V alloy. In Ti–6Al–4V, Al is α phase stabilizer while V is beta stabilizer.
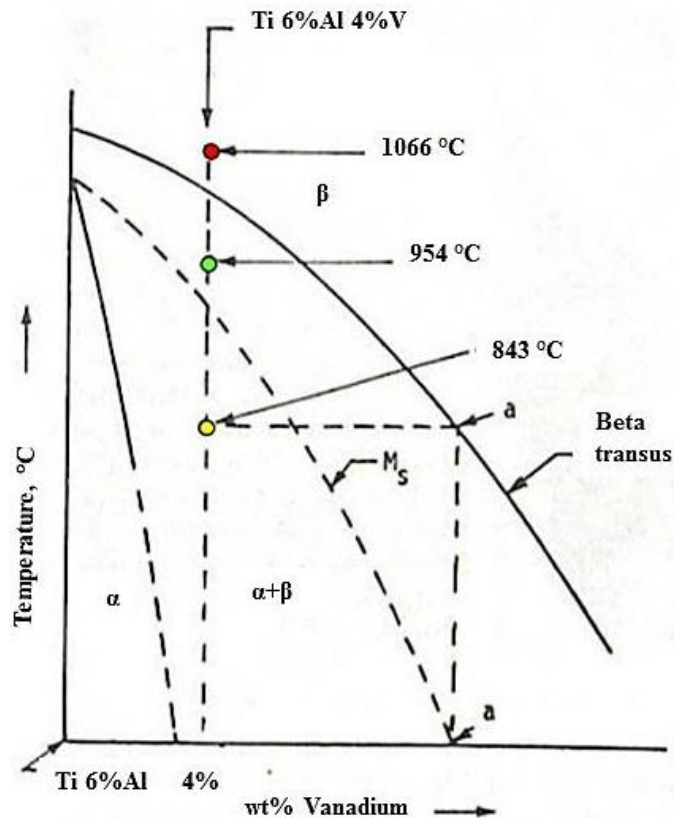
Fig. 1.7 Schematic phase diagram of Ti–6Al with varying content of V (MS: martensite start temperature) [Leyans et al. (2003)].

1.3.4.1 Microstructure of Alloy Ti–6Al–4V (α+β alloy)

The microstructure of the alloy Ti–6Al–4V is strongly dependent on heat treatment processing and it can be described by size and arrangement of α and β phases [Gammon et al. (2003)]. The microstructures of Ti–6Al–4V (α+β titanium alloy) are of three different types: (1) fully lamellar, (2) fully equiaxed, and (3) bi-modal (or dual phase) containing equiaxed primary α in a lamellar α+β matrix [Lutjering et al. (2003)]. The chemical compositions of the α and β phases change in the two-phase field with decreasing temperature under equilibrium conditions.

1.3.4.1.1   Fully Lamellar Microstructure

Fully lamellar microstructure is obtained by heating of the sample above β transus, followed by slow cooling. The cooling rate from the β solution treatment temperature is important because it determines the final lamellar structure and the thickness of the α layer at β grain boundaries. Therefore, lamellar structures depend on the cooling rate and the lamellae could be fine or coarse controlled by the rate of cooling. When the cooling rate is slow from the β phase field, fully lamellar microstructure results (Fig. 1.8a). However, air cooling leads to a martensitic transformation of β, resulting in a very fine needle-like microstructure (Fig. 1.8b) [Humphreys et al. (2004), Vander (2004)].
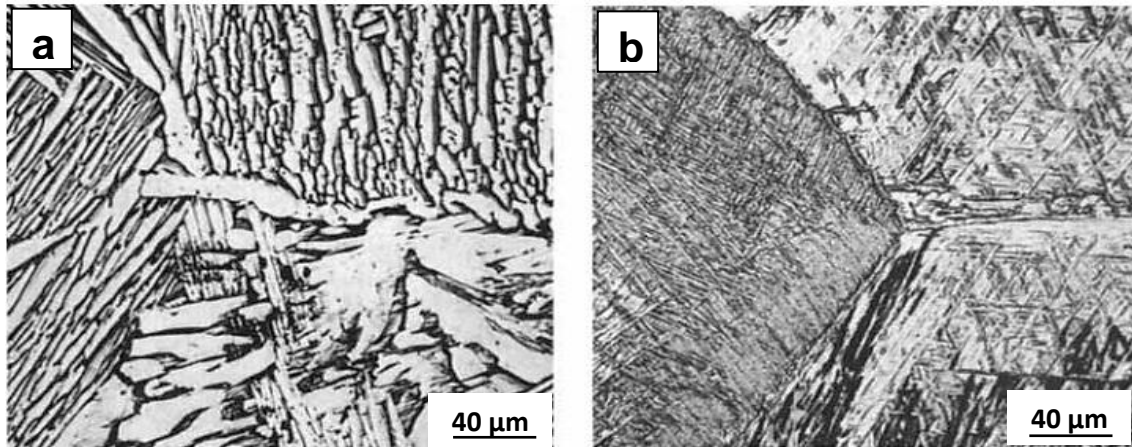
**Fig. 1.8** Ti–6Al–4V alloy, held for 1h at 1065 °C, above the beta transus (a) furnace cooled, (b) air cooled [Vander (2004)].

1.3.4.1.2   Fully Equiaxed Microstructure

Equiaxed microstructures result from the process of recrystallization. Therefore, the alloy is first deformed in the α+β field to introduce enough cold work into the material. Consequent, solution heat treatment at temperatures in the α+β phase field

results in recrystallized and equiaxed microstructure (Fig. 1.9a). Extended annealing coarsens the equiaxed microstructure (Fig. 1.9b). The solution heat treatment temperature determines the volume fraction of the primary α [Lutjering (2003)]. It is obvious that cooling from the α+β phase field produces microstructure approaching equilibrium equiaxed primary α phase surrounded with retained β phase. Figure 1.9 shows the equiaxed microstructure of Ti–6Al–4V alloy.
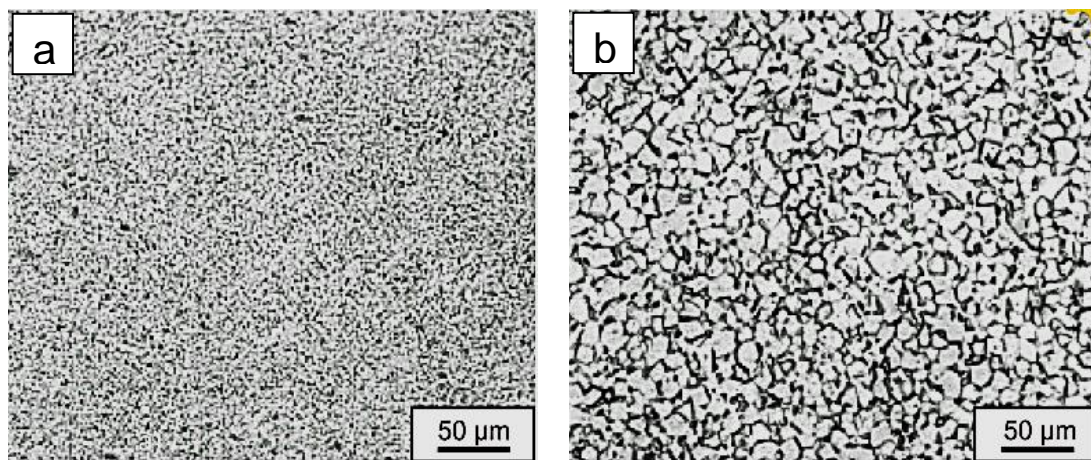
**Fig. 1.9** Equiaxed microstructures of alloy Ti–6Al–4V via recrystallization: (a) fine equiaxed, (b) coarse equiaxed [Leyans et al. (2003)].

1.3.4.1.3   Bi-modal (dual phase) Microstructure

A bi-modal microstructure can be produced through solution heat treatment. When the α+β titanium alloys are treated below the β transus temperature a bimodal microstructure results, which consists of globular primary α and transformed β. It may be seen from Fig. 1.10a that the microstructure consists of equiaxed α grains (light) and the dark regions of transformed β. In, Fig 1.10b structure is similar to that in (Fig. 1.10a); however, the faster cooling results in finer acicular alpha in the transformed beta (Fig. 1.10b). The stability of bi-modal structure depends on the volume fraction of

primary α and transformed β phases. Some α+β alloys with their properties and applications are recorded in Table 1.4.
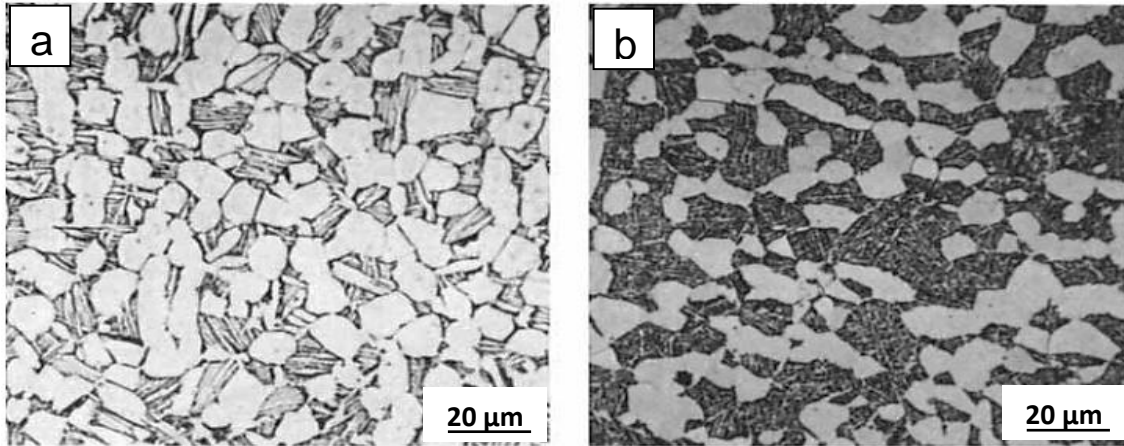
Fig. 1.10 Ti–6Al–4V alloy solution treated for 1h at 955 °C: (a) air cooled, and annealed for 2h at 705 °C, (b) water quenched [Vander (2004)].

Table 1.4 α+β titanium alloys and their applications [Polmer (2006), Leyans et al. (2003)].

| S. No.	Alloy	Applications	Tensile strength	
			YS (MPa)	UTS (MPa)
1.	Ti–6Al–4V	aerospace engine, chemical industries and medical devices	800-1100	900-1200
2.	Ti–6Al–6V–2Sn	aerospace structures	950-1050	1000-1100
3.	Ti–6Al–2Sn–4Zr–6Mo	gas turbine engine components	1000-1100	1100-1200
4.	Ti–6Al–2Sn–2Zr–2Mo–2Cr–0.25Si	landing gear	1000-1200	1100-1300

1.4 SURFACE MODIFICATION TECHNIQUES

Surface properties of structural components have been improved by various surface modification processes such as laser shock peening, conventional shot peening, ultrasonic shot peening and high energy shot peening. These techniques could be highly effective in enhancing corrosion resistance and fatigue life of structural components from the combined effect of surface grain refinement and the associated compressive residual stresses in the surface and subsurface regions, by delaying the process of crack initiation and the initial crack propagation.

Among the different processes of surface modification, ultrasonic shot peening is a relatively new process of generating surface nanostructure. It has high potential for improving mechanical properties of metals and alloys without changing their chemical compositions [Sanda et al. (2011)].

1.4.1 Laser Shock Peening

Laser shock peening or laser peening is a surface engineering process used to improve fatigue strength and corrosion resistance. The compressive residual stress induced by laser peening increases the resistance of materials to surface related failures, such as fatigue and corrosion [Shadangi et al. (2015)]. During this process, metal part is struck by a high energy pulsed laser beam producing high amplitude stress waves. Laser shock peening process parameters are shown in Fig. 1.11. The surface of the material resists stretching induced by the stress waves and results in formation of a compressed skin. Various parameters are used for laser peening such as laser wavelength of about 1 μm, pulse duration 10-50 nanoseconds, pulse energy 50-100 joules and beam diameter 5 mm.
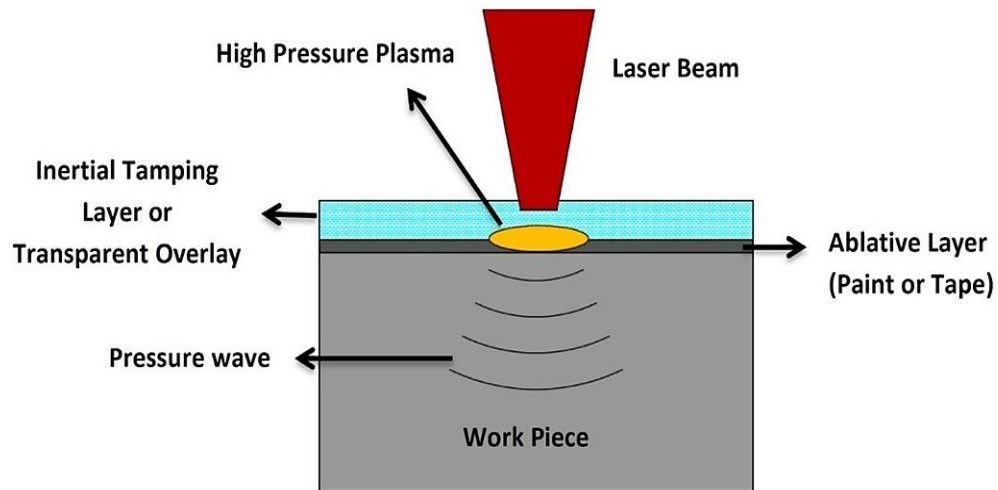
Fig. 1.11 Process parameters for laser shock peening [Abdullahi et al. (2014)].

Laser shock peening produces compressive stress approximately 4 to 5 time deeper in the materials than that from shot peening. The compressive residual stress prevents both crack initiation and propagation. Therefore laser peening is used mainly for increasing fatigue strength due to deeper penetration of the compressive stress.

Laser shock peening has been applied to a variety of alloys used in aircraft engines, airframes, and other engineering applications. Laser shock peening has been applied successfully to improve the damage tolerance of several critical compressor blade leading edges and has made major contributions to the field of surface enhancement [Charles et al. (2002)].

1.4.2 *Conventional Shot Peening (SP)*

Conventional shot peening is a cold work process used to produce grain refinement associated with compressive residual stress which improve mechanical properties of metals/alloys and composites. SP equipment is schematically shown in Fig. 1.12. In this process, small spherical shot media (metallic, glass, or ceramic) with sufficient hardness are accelerated in peening device of various kinds and impact on the surface

of the material with energy to create plastic deformation. The main benefit of shot peening is the delay in crack initiation in highly tensile stressed alloy components due to grain refinement associated with compressive residual stresses close to the surface region. These effects are very useful in preventing the failure of materials due to corrosion and fatigue. Among various types of shot peening, air blast shot peening (ABSP) is known as conventional shot peening [Umemoto et al. (2005)].
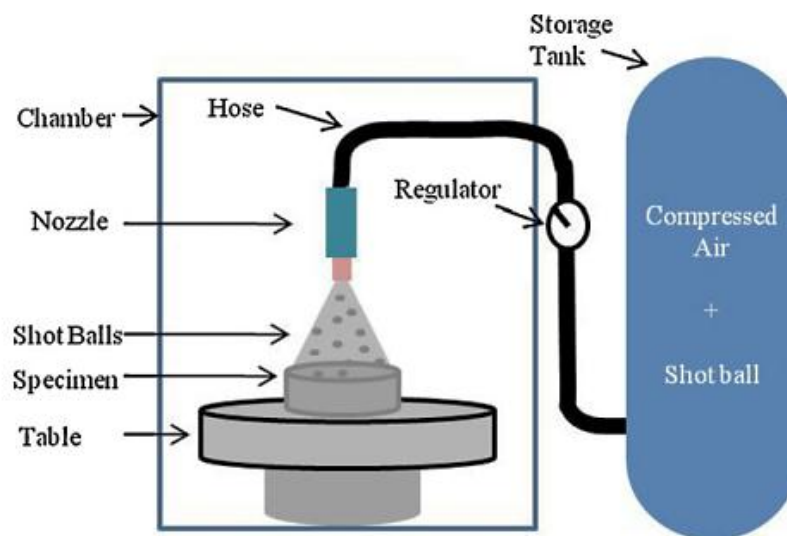
Fig. 1.12 Schematic diagram of shot peening process [Cho et al. (2012)].

1.4.2.1 Air Blast Shot Peening (ABSP)

ABSP is a shot peening process, in which shots are projected by compressed air and through nozzle onto the component. The schematic diagram of the equipment in conventional operation is shown in Fig. 1.13. In this process, the shot velocity is maintained >100 m/s and the impact direction of shot to specimen is almost perpendicular [Todaka et al. (2004)].
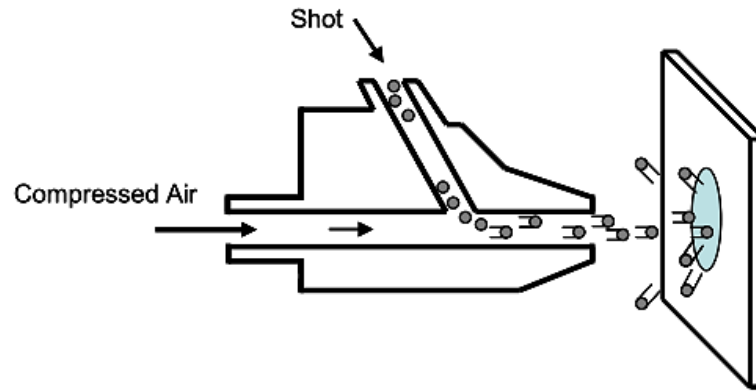
Fig. 1.13 Schematic illustration of the equipment of air blast shot peening [Umemoto et al. (2005)].

1.4.3 Ultrasonic Shot Peening (USSP)

The surface nanostructuring by USSP is a new methodology of surface modification to improve the performance of structural components. USSP is also known as surface mechanical attrition treatment (SMAT) process and is based on the same principle as the conventional shot peening. The main differences between the conventional shot peening and USSP are recorded in Table 1.5. USSP is a cold working process performed at room temperature in which the surface of work-piece is subjected to impact of small balls, at ultrasonic frequency and causes severe plastic deformation. The balls are projected against the surface being peened. Steel balls impacting on the surface of the material create dimple and associated compressive residual stress as shown in Fig. 1.14.

Different microstructures from nano to sub-micron size are produced in surface region using this method. USSP induces a low roughness and a better surface quality compared to the conventional shot peening. The parameters to check in order to control the crack initiation effect on the subject are: treatment time, mass of the balls in the housing, sonotrode vibration amplitude. Those parameters are computer controlled and

allow the reproducibility of the procedure. The USSP system consists of an acoustic assembly with piezoelectric transducer, booster and sonotrode. The acoustic assembly creates mechanical vibration and transmits it to set steel balls in motion. Piezoelectric transducer emits ultrasonic waves at 20 kHz and the waves are amplified while traveling through an acoustic booster, in a housing holding the sample to be treated and the balls for peening. The system of USSP is shown in Fig, 1.15.

Table 1.5 The basic difference in between SP and USSP [Cho et al. (2012), Mitsubishi (2011)].

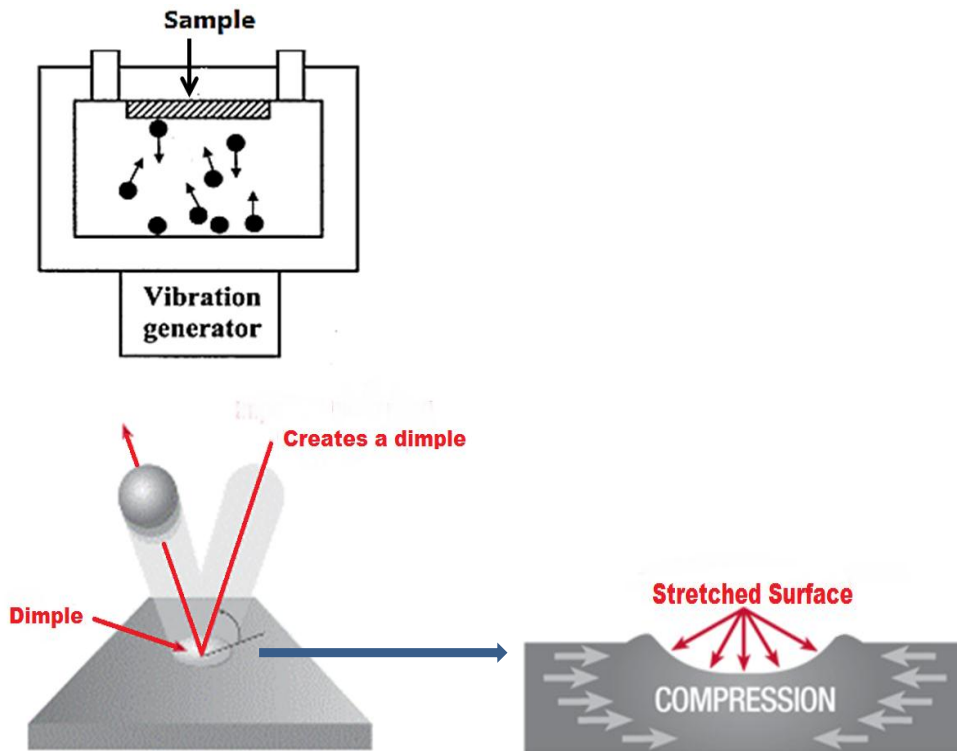| S. No.	Parameters	SP	USSP
1.	Balls size	0.25 mm to 1 mm	1 mm to 8 mm
2.	Velocity	20 m/s to 150 m/s	3 m/s to 20 m/s
3.	Frequency	50-200 Hz	20 kHz
4.	Roughness	Higher	Lower
5.	Compressive residual stress	Lower depth of compressive stresses	Higher depth of compressive stresses

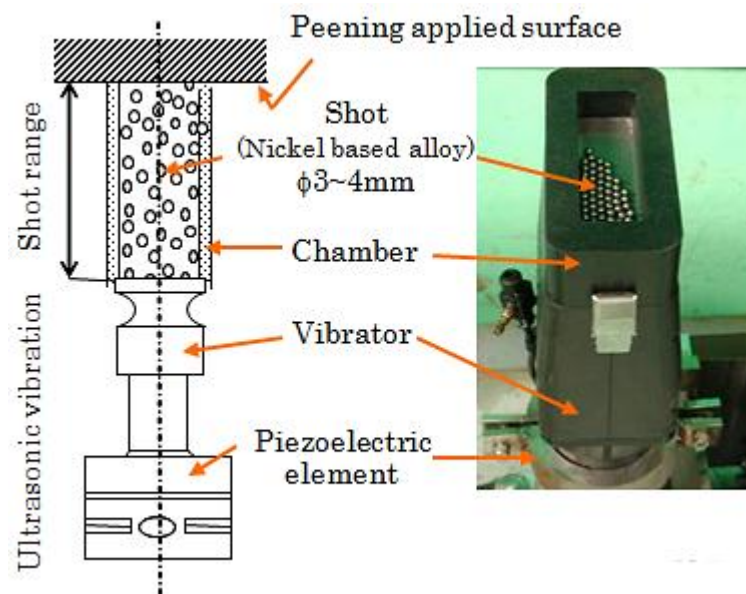**Fig. 1.14** Principle of ultrasonic shot peening [www.globalspace.com].

Fig. 1.15 Schematic representation of ultrasonic shot peening [Mitsubishi (2011)].

1.4.4 High Energy Shot Peening

High-energy shot peening is another method reported to be capable of synthesis of nanostructured surface layers. The principle of the high-energy shot peening treatment is similar to surface mechanical attrition, but with lower frequency and bigger shots. Similar to previous methods, the entire surface of the sample to be treated is peened by flying shots with a high energy and nanocrystalline layer is achieved using different durations for peening [Bagherifarda et al. (2010)]. High energy shot peening is one of the effective processing for the manufacture of various ultrafine-grained structures by imposing intense plastic strains onto the surface of the metals and alloys. The plastic strain present shows gradient distribution in the surface layer, changing from the maximum at the top surface to near zero far into the matrix. The microstructure observation at various depth levels can, therefore, provide the clue to the process of structural evolution relevant to various stages of strain [Feng et al. (2008)].

1.5   EFFECT OF USSP ON MICROSTRUCTURE

Surface nanostructure is produced through severe plastic deformation in surface region for commercial structural applications. Surface nanostructured components have high wear resistance, fatigue resistance, and good corrosion resistance. Surface nanostructure induced by ultrasonic shot peening has been studied by several researchers in different materials. Nanostructure has been reported to a depth of 20 μm in pure iron [Tao et al. (1999, 2002), Guo et al. (2004, 2006)]. Effect of ultrasonic shot peening has been studied in 316L stainless steel and low carbon steel, using small shots of 3 mm diameter for different durations of 30, 60, 90 and 810 seconds. In all the cases there was grain refinement in surface layer of the processed specimen and nanostructure was observed up to a depth of 30 μm [Liu et al. (2000, 2001)]. Nanocrystalline surface

layers have been reported in 321 stainless steels [Mordyuk et al. (2007)], aluminium alloys [Wu et al. (2002)], Ni-base alloy 600 [Tao et al. (2004)] and Ni-base alloy C-2000 alloy [Villegas et al. (2005, 2009)]. It was concluded that the mechanism responsible for surface grain refinement was severe plastic deformation with high dislocation activity and deformation micro-twins.

Zhu et al. (2004) and Wen et al. (2008, 2009) observed nanostructure of ~50 nm and ~30 nm respectively in cp–titanium resulting from USSP. Zhu et al. (2004) have reported nanostructure of 50 nm in α titanium from USSP (Fig. 1.16).
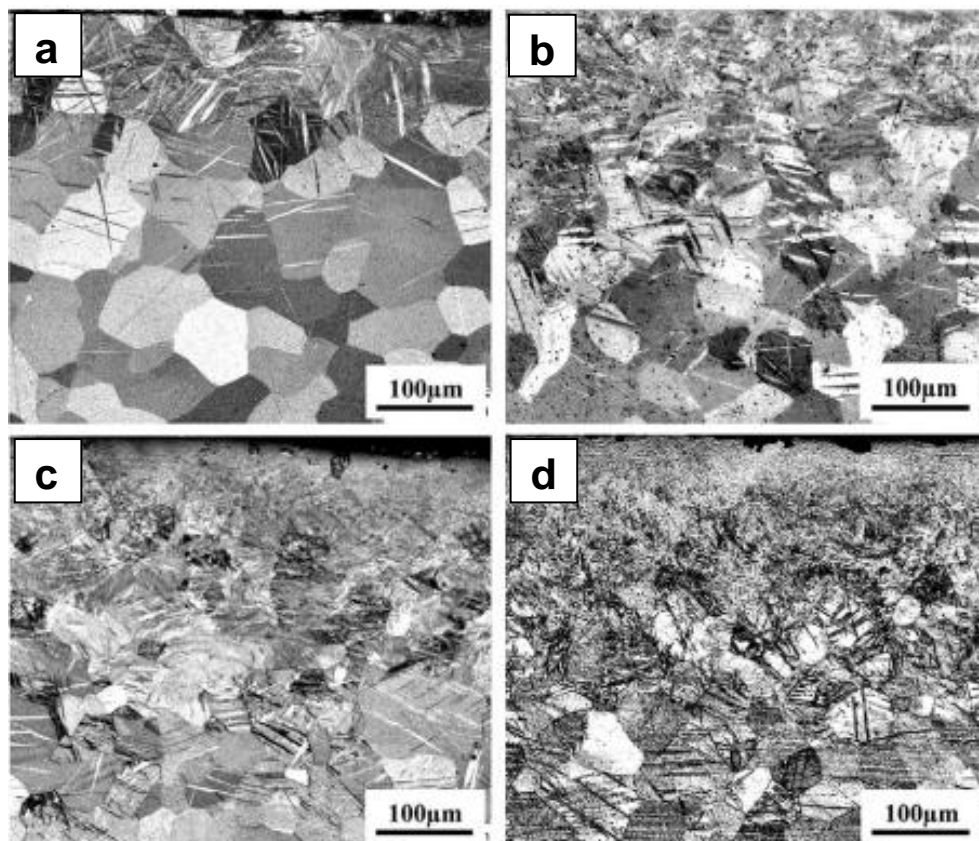
Fig. 1.16 Cross-sectional optical micrographs of cp-Ti close to the SMAT-treated surfaces under different conditions: (a) 10 minute, (b) 16 minute, (c) 30 minute and (d) 60 minute [Zhu et al. (2004).

Lei et al. (2014) observed nanostructure of 10 to 30 nm size in β type titanium alloy Ti–Nb–Zr–Fe up to a depth of 30 μm resulting from USSP. Jelliti et al. (2013) studied effect of USSP on grain refinement in surface region of Ti–6Al–4V alloy for 15 and 20 minute USSPed specimens using balls of 2 and 3 mm diameters, respectively. Grain refinement was found to be more with the ball of 3 mm diameter than that of 2 mm diameter.
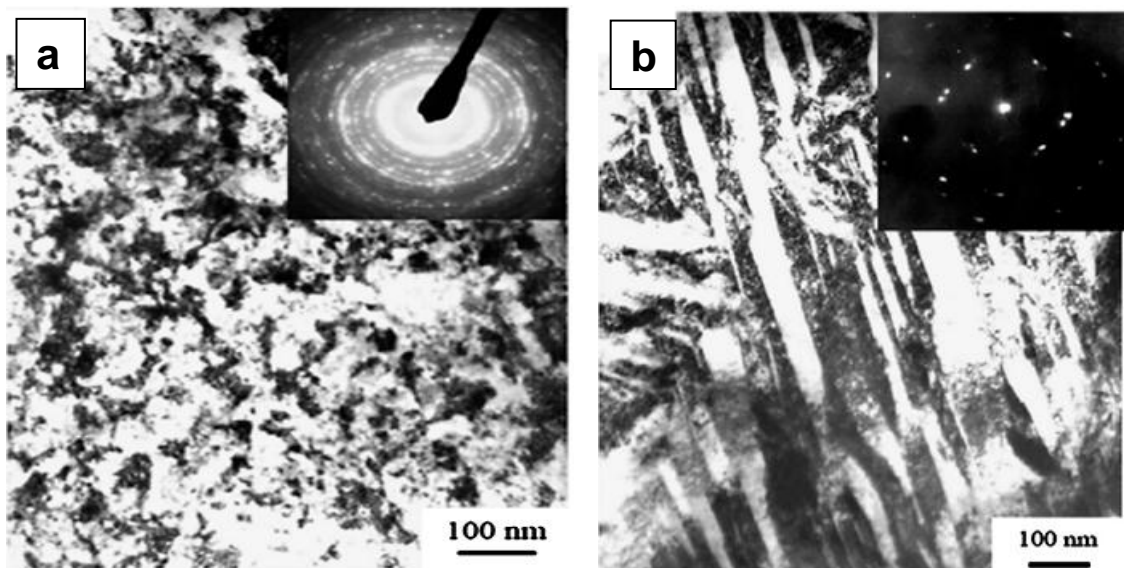
Fig. 1.17 Bright field TEM micrographs with corresponding SAD patterns at the depth of (a) 5 μm (b) 20 μm from the surface of alloy Ti–6Al–4V following USSP with 3 mm balls diameter [Jelliti et al. (2013)].

It may be seen from Fig. 1.17 that there are typical ring shaped SAD patterns of a fine structure, with random crystallographic orientations. Nano size grains were observed with an average size of 50 nm. However, grain size varied with depth from the treated surface (Fig. 1.17). The mechanism of grain refinement involves a high twinning activity that subdivides coarse grain into nanograins. The formation of nanograins can be attributed to the large distortions and strain rates during the treatment, as well as multidirectional impacts which promote the activation of several

twinning systems. Meng et al. (2011) and Tao et al. (2004) proposed that twinning plays important role in grain refinement. Micro-twinning has been found to be more important in case of low stacking fault energy materials.

1.6 EFFECT OF USSP ON CORROSION

Corrosion can be defined as degradation of a material due to a reaction with its environment. Degradation indicates deterioration of physical properties of the material. Most corrosion of materials is electrochemical in nature. Therefore, Ti–6Al–4V fails due to corrosion; like stress corrosion, electrochemical corrosion and hot corrosion (at elevated temperature). Electrochemical corrosion is one of the failure modes of titanium based implant alloys. The failure of alloy Ti–6Al–4V implant prosthetic component may be caused by the interaction of electrochemical corrosion and mechanical wear mechanism in the biological corrosive environment.

Degradation of materials in the marine environment at high temperature is known as hot corrosion. Rapid degradation occurs due to lack of a solid protective layer on the substrate. Components that are affected by hot corrosion attack include gas turbines, industrial plants, and jet engines. Therefore, materials degrade resulting from hot corrosion.

1.6.1 *Electrochemical Corrosion*

Electrochemical corrosion is one of the most significant phenomena which occur for biocompatible metals/alloys used as implants in the body [Redamond et al. (1982), Park et al. (1992)]. Because of the high concentration of chloride ions (Cl^-) and temperature range of the body, the human body fluid is considered as a severe corrosive environment [Yang et al. (2013)]. Titanium and titanium alloy are used as medical

implants in the human body mainly for orthopedic purposes [Wen et al. (2007), Budi et al. (2013)]. They are widely used in various shapes as implants in humans. Therefore, they must have the required mechanical resistance and good corrosion resistance.

As discussed earlier, Ti–6Al–4V is an important α+β type alloy and is widely used as the material for orthopedic and dental bio-implants because of its excellent corrosion resistance, high strength, and biocompatibility. It is best suited for implants because of its high strength and formation of passive film on the surface [Gurappa (2002), Kobayashi et al. (2006)]. The Ti–6Al–4V alloy has excellent corrosion resistance in physiological environments due to the formation of a protective oxide layer of TiO_2 (rutile) [Li et al. (2010), Hsu et al. (2004)].

Various surface modification processes have been used to increase the corrosion resistance of metals and alloys such as coating, laser shock peening, shot peening and ultrasonic shot peening. Li et al. (2010) reported that corrosion resistance was improved by a nanostructured Al_2O_3-TiO_2 coating onto Ti–6Al–4V. However, Balakrishnan et al. (2008) studied corrosion behavior of ultrafine grained cp-Ti, in body fluid. The ultrafine grains were produced through equal channel angular process. Yue et al. (2002) reported that laser surface treatment significantly improved the corrosion resistance of the alloy Ti–6Al–4V. The improvement was considered to be primarily due to the reduction of the solute partitioning effect of detrimental Al, which segregates to the α phase. Shadangi et al. (2015) also studied corrosion behavior of interstitial free steel in the aqueous solution of 3.5% NaCl with 5 minute overlapping of laser shocks and reported that corrosion resistance of single laser shock peened interstitial free steel was higher than that of the overlapped laser shock.

Wang et al. (2006) have studied corrosion behavior of the surface nanocrystalline microstructure of 1Cr18Ni9Ti stainless steel. The nanocrystalline microstructure was induced by conventional shot peening. Jindal et al. (2014) studied corrosion behavior on the surface nanostructure of cp-Ti, using ultrasonic shot peening. USSP is the latest and a unique process for improving the corrosion resistance of metals and alloys. Several investigators have studied corrosion behaviour of nanocrystallized materials. Balusamy et al. (2010) compared corrosion behavior of surface nanocrystallized AISI 409 stainless steel, following USSP for 15, 30 and 45 minute with stainless steel balls of 2, 5 and 8 mm diameter and observed that corrosion resistance was improved from USSP with 2 mm balls for 15, 30 and 45 minute but was reduced from USSP with 5 and 8 mm balls for 5, 30 and 45 minute.

Lei et al. (2014) studied corrosion behavior on nanostructured surface of the alloy Ti–Nb–Zr–Fe and found that corrosion resistance was improved on the nanocrystallized surface from rapid formation of a passive film. Garbacz et al. (2007) reported that nanostructuring of cp-Ti caused lowering of corrosion resistance in 0.9% NaCl solution as compared to that of the coarse grained material. Raducanu et al. (2011) developed nanostructure in Ti–Zr–Ta–Nb alloy by rolling and observed that corrosion resistance was improved due to nanostructuring. Huang et al. (2013) studied effect of USSP on corrosion behavior of nanostructured Ti–25Nb–3Mo–3Zr–2Sn alloy in NaCl and Ringer solution, and observed lower rate of corrosion due to grain refinement. Jelliti et al. (2013) studied effect of ultrasonic shot peening on grain refinement in Ti–6Al–4V alloy, following USSP for 15 and 20 minute with balls of 2 and 3 mm diameters respectively. Since there was variation, both in the time of USSP as well as the ball diameter, it is difficult to visualize the effect of the individual variable. However, corrosion resistance was improved due to USSP.

1.6.2 High Temperature Oxidation

Oxidation is one of the major factors limiting the life of titanium alloys in gas turbine engine components like compressor discs and blades of advanced gas turbine engines of light weight aircraft. Their degradation is due to gaseous environments, in particular, the one containing oxygen, especially at elevated temperatures, during the long term use.

They suffer from extensive scaling when exposed to oxidizing environment mostly at relatively high temperatures [Kofstad et al. (1988)]. Exposure of titanium and its alloys to any oxygen-containing atmosphere at elevated temperatures leads to formation of an oxide layer on the surface with an oxygen diffusion zone beneath it. Rutile and anatase are the most common modifications of TiO_2 that form an oxide layer. Irreversible anatase to rutile phase transition takes place within the oxide layer at about 700 °C [Gryorgy et al. (2007)]. Dissolution of oxygen in the substrate as a result of inward diffusion of oxygen causes the development of hard and brittle oxygen diffusion zone. Since it leads to a loss of tensile ductility and of fatigue resistance, oxygen diffusion zone formation is critical to the life expectancy of titanium alloys, for example when used in aero-gas turbine engines [Gurrappa (2005)]. The addition of aluminum considerably enhances the oxidation resistance of titanium by forming thermodynamically stable, protective α-Al_2O_3 phase. If aluminum content is sufficient, the oxide layer will be composed of a mixture of TiO_2 and α-Al_2O_3 [Becker et al. (2004)].

1.6.3 Hot Corrosion

Hot corrosion may be defined as an accelerated corrosion, resulting from the presence of salt contaminants such as Na_2SO_4, $NaCl$, and V_2O_5 that combine to form

molten deposits, which damage the protective surface oxides. Titanium alloys are affected by hot corrosion attack in gas turbine components. In a gas turbine engine, NaCl from the air reacts with sulphur from the fuel to form Na_2SO_4. The sulphate then deposits on the hot sections like turbine blades, resulting in accelerated oxidation. The little amount of sulphur present in low-grade fuel is sufficient to cause corrosion. Titanium alloys that suffer from hot corrosion attack exhibit both sulfidation and oxidation. The deposit of the molten sodium sulphate is responsible for the initiation of hot corrosion attack. There are two types of hot corrosion: (1) high-temperature hot corrosion (2) low-temperature hot corrosion.

1.6.3.1 High Temperature Hot Corrosion

High temperature hot corrosion is nominally observed in the temperature range of about 800-950°C, because pure sodium sulphate melts above this temperature. It is an extremely rapid form of oxidation that takes place at this range of temperatures in the presence of sodium sulphate. Other impurities either in the fuel or in the air, such as vanadium, phosphorus, lead and chlorides combine with sodium sulphate to form a mixture of salts with a lower melting temperature, thus broadening the range of attack. Potassium sulphate acts similar to sodium sulphate in respect to high temperature hot corrosion [Eliaz et al. (2002)]. Sulphur is released by the reduction of sodium sulphate. The sulphur diffuses inward and then reacts with aluminium/chromium from the substrate to form aluminium/chromium sulphides. As corrosion proceeds, and phase stability adjusts to changing chemistry, the sulphides are converted to complex unstable metal oxides and the sulphur thus released diffuses more deeply into the substrate where it forms more sulphides [Koul et al. (1993)].

1.6.3.2 Low Temperature Hot Corrosion

Low-temperature hot corrosion occurs below the melting point of pure Na_2SO_4. It takes place at temperatures in the 593-760 °C range and requires a significant partial pressure of SO_3. It is caused by low melting eutectic compounds resulting from the combination of sodium sulphate and some of the alloy constituents such as titanium. This corrosion is rarely observed in aero-engines because the blades are generally operated at higher temperatures [Koul et al. (1994)]. This type of hot corrosion occurs in marine and industrial gas turbines. Low-temperature hot corrosion generally proceeds in two stages: an incubation period exhibiting a low corrosion rate, followed by accelerated corrosion attack. The incubation period is related to the formation of a protective oxide scale. Initiation of accelerated corrosion attack is related to the breakdown of the protective oxide scale.

Many mechanisms have been proposed to explain accelerated corrosion attack; the salt fluxing model is probably the most widely accepted. Oxides can dissolve in Na_2SO_4 as anionic species (basic fluxing) or cationic species (acid fluxing), depending on the salt composition [Meier (1989)]. Salt is acidic when it is high in SO_3, and basic when low in SO_3.

Hot corrosion failure is a big issue for degradation of materials because this alloy is commercially used for aerospace engine components at elevated temperature applications with superior mechanical strength, corrosion resistance, and fatigue resistance [Leyens et al. (2003)]. However, above 400 °C, it oxidizes rapidly in the oxygen-containing environments and also undergoes hot corrosion in the marine environment. Low-grade fuel oils cause hot corrosion, forming Na_2SO_4 and V_2O_5 during combustion. Na_2SO_4 is produced from the reaction of NaCl in air and sulphur

(present as impurity) in the fuel oil. Vanadium in the fuel oil in the form of vanadium porphyrin transforms into V_2O_5 during combustion [Mahobia et al. (2013)]. Kamal et al. (2015) purposed that V_2O_5 and Na_2SO_4 form low melting inorganic compounds which undergo eutectic reaction below 600 °C.

Effect of surface nanostructure has been studied also on oxidation behavior of titanium and its alloys. Tan et al. (2008) reported the effect of shot peening on the oxidation behavior of alloy 800H at 850 °C and found that the corrosion resistance was improved following shot peening. Wen et al. (2012) studied oxidation behavior of cp-Ti at 500, 600 and 700 °C with USSP and observed that oxidation resistance was improved following USSP.
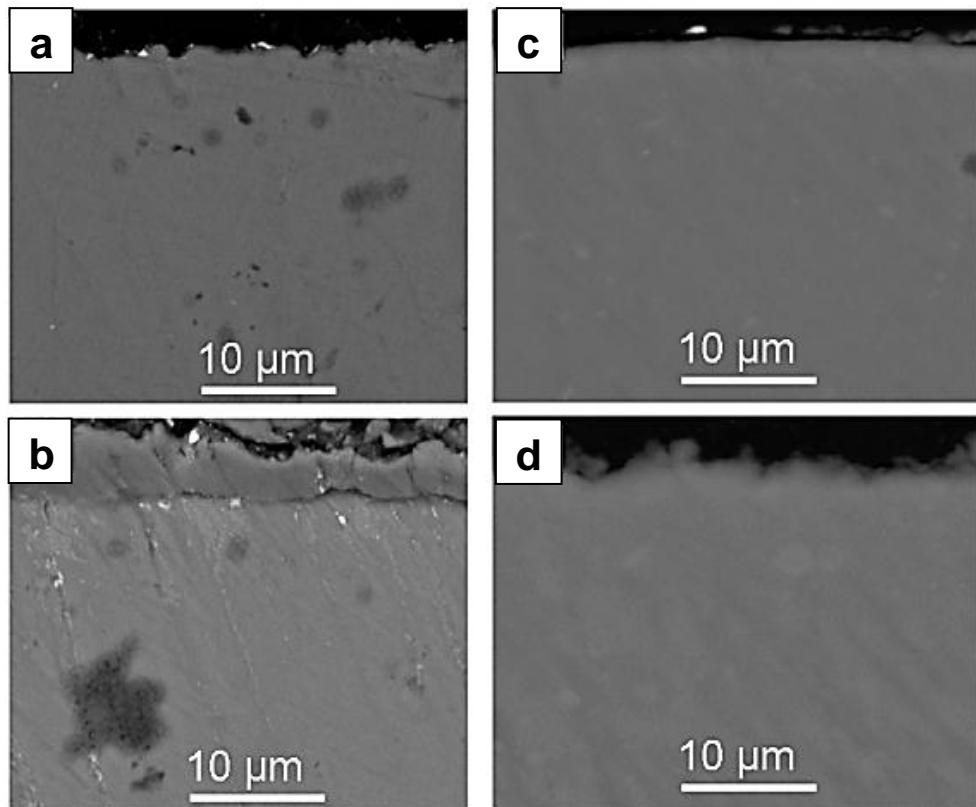
**Fig. 1.18** Cross-sectional morphology of cp-Ti oxidised layer on USSPed sample at (a) 500 °C, (b) 600 °C and non-USSPed at (c) 500 °C, (d) 600 °C [Wen et al. (2012)].

Oxidised layer was not visible at 500 °C for the non-USSPed and USSPed sample. However, the thickness of the oxidized layer increases with increase in temperature (Fig. 1.18). It is also obvious that the oxidised layer of the USSPed sample is much denser than the porous oxide layer in the non-USSPed. Similar improvement in oxidation resistance has been reported also in zirconium by Zhang et al. (2007) from surface nanostructuring. Oxidation behavior of the high-temperature near-α titanium alloy Ti metal 834 and alloy Ti–6Al–4V have been studied earlier [Srinadh et al. (2007), Frangini et al. (1994)]. The rate of oxidation and thickness of oxide scale at different temperatures was found to be proportional to the temperature of exposure.

Hot corrosion behavior of the high-temperature titanium alloy Ti metal 834 was studied at 500-700 °C in different salt mixtures and maximum deterioration was observed in corrosion resistance in the salt mixture containing V_2O_5 [Gurrappa (2003)]. A similar observation was made also for hot corrosion of the alloy Ti–6Al–4V in different salt environments, in air, Na_2SO_4–60%V_2O_5 and Na_2SO_4–50%NaCl at 750 °C [Mahesh et al. (2007)]. It was observed that corrosion rate of the alloy Ti–6Al–4V was relatively high in the molten salt environment when compared to that in air. The corrosion rate of alloy Ti–6Al–4V was in the following order: air<Na_2SO_4–50%NaCl<Na_2SO_4–60%V_2O_5 (Fig. 1.19). The degradation of material occurs due to the chemical reactions between titania and chloride ions, sulphur and vanadium present in the environment.

However, no information is available on the effect of ultrasonic shot peening and the resulting surface nanostructure on hot corrosion behavior of titanium and its alloy.
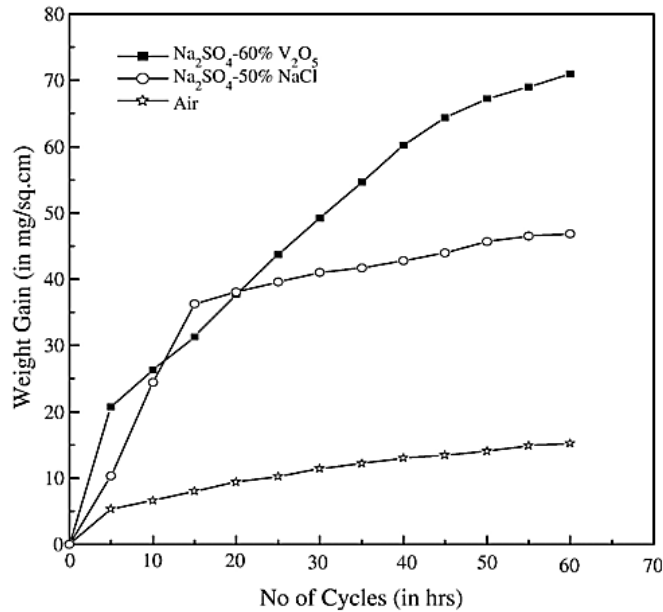
Fig. 1.19 Weight gain versus number of cycles for the Ti–6Al–4V samples subjected to cyclic oxidation in air, Na_2SO_4–60% V_2O_5 and Na_2SO_4–50% NaCl at 750 °C [Mahesh et al. (2007)].

1.7   EFFECT OF USSP ON FATIGUE LIFE

Most of the failures of structural components arise from cyclic loading and initiation of cracks from the surface. Also the process like fretting fatigue is highly sensitive to surface characteristics of the material. Low cycle fatigue (LCF) occurs in aerospace gas turbine components from start-up and shut down operation. LCF is the main reason for cycle limitations on component life. LCF is related to the much higher stress cycles imposed by starting and stopping operations. In the gas turbine, the disks which hold the blades in an engine are commonly life limited by the number of stop/start cycles to which they are subjected to in service, rather than by the hours of service. This rate varies considerably depending on the engine, and is determined largely by the size of the loadings imposed and the temperatures to which the disk is exposed.

Several investigators have reported that alloy Ti–6Al–4V has higher fatigue strength in the dual phase microstructure, with globular primary α and transformed β, as compared to the basketweave microstructure [Wu et al. (2013), Zuo et al. (2008)]. Peters et al. (1990) and Lutjering et al. (1994) also reported that bi-modal microstructure has good mechanical properties such as yield strength, tensile strength and ductility and fatigue strength than the lamellar structure (Fig. 1.20). Therefore, bi-modal microstructure is selected for disk of gas turbine engine because of the much better low cycle fatigue and high cycle fatigue strength and micro-crack propagation resistance as compared to the fully lamellar microstructure [Lutjering et al. (2003)].
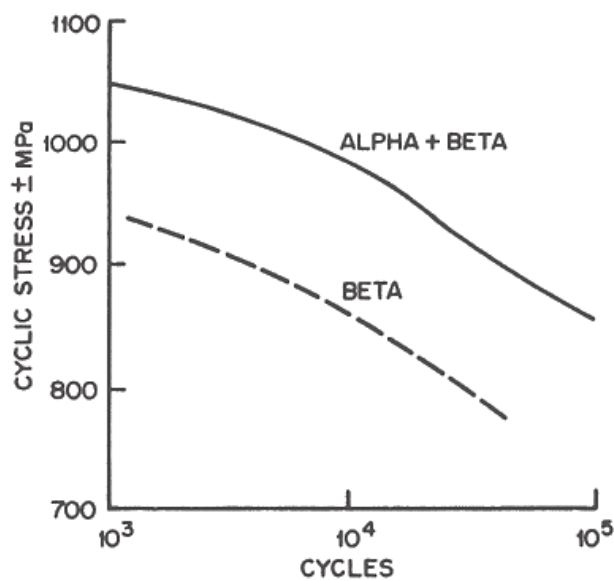
Fig. 1.20 Comparison of low-cycle fatigue life of Ti–6Al–4V in mill-annealed and β-annealed condition [Lutjering et al. (1985)].

The high cycle fatigue strength is deepening resistance to crack nucleation, which depends primarily on the first dislocation motion. However, LCF strength depends on both, the resistance to crack nucleation and the resistance to propagation of the small surface cracks (micro-cracks) [Lutjering (1998)].

Fatigue failure of structural components originates from the surface or subsurface, therefore it is essential to implement a process which is not only cost effective but also produces a high quality of surface in the successive processes of manufacturing. This alloy has higher fatigue strength in the dual phase microstructure, with globular primary α and transformed β, as compared to the basketweave microstructure [Zuo et al. (2008), Wu et al. (2013)]. Alloy Ti–6Al–4V is prominently used as prosthesis in medical applications. Most of the physical activities like walking, running, talking etc. create conditions similar to those found in fatigue failure of prosthesis.

Mostly fatigue cracks initiate from the surface and propagate to interior. Component with nanostructured surface layer is predicted to have highly improved fatigue strength because of enhanced resistance against fatigue-crack initiation and propagation. Therefore, improvement in fatigue resistance of such components is quite important. Moreover, the residual compressive stresses introduced in the surface region during USSP also effectively reduce the initiation and propagation of fatigue cracks [Teoh et al. (2000)]. Moreover, the conventional shot peening of such components is likely to produce highly rough surface in comparison to that obtained after USSP. The surface roughness leads to reduction in fatigue life of the material [Milan et al. (2013)].

Further, surface roughness also plays an important role in osseo-integration and life of dental implant made of alloy Ti–6Al–4V [Nektarios et al. (2009)]. Thus, USSP is likely more effective than conventional shot peening in improving fatigue resistance. However, little attention has been paid on the effect of USSP on other aspects.

Surface properties of structural components have been improved by various surface modification processes such as surface coating [Yong et al. (2014)], shot peening [Gray et al. (1986), Liu et al. (2007)], laser shock peening [Igor et al. (2012),

Lin et al. (2014)], and ultrasonic shot peening [Chattopadhyay et al. (2014), Rai et al. (2014)]. These techniques could be highly effective in enhancing fatigue life of structural components from combined effect of surface grain refinement and the associated compressive residual stresses in the surface and subsurface regions, by delaying the process of crack initiation and the initial crack propagation. The compressive residual stress fields associated with USSP remain confined to short depth of nearly 0.25 mm [Prevey et al. (2005), Charles et al. (2002)].

Lee et al. (2006) found that fretting fatigue life of Ti–6Al–4V was improved from shot peening in the region of the both high and low cycle fatigue under sea water environment. Fatigue strength of shot-peened Ti–6Al–4V was decreased with increase in the temperature of stress relieving from 100 ℃ to 260 ℃ [Lee et al. (2004), (2005)]. Similar observation was made also by Xiaohua et al. (2009) on the shot peened titanium alloy Ti811 resulting from annealing at 350 ℃ and 500 ℃ for 100h and 1h respectively. Fatigue strength of the alloy Ti811 was increased from annealing at 350 ℃, however, it was decreased following annealing at 500 ℃ because of the lower compressive residual stress associated with the specimen, annealed at the higher temperature of 500 ℃.

Rai et al. (2014) studied LCF on high-nitrogen austenitic stainless steel with USSP, using steel balls of 3 mm for 10 minute and found negative result on fatigue life at lower strain amplitude. However, LCF life was almost same for non-USSPed and USSPed at high strain amplitude of ±1.0% (Fig. 1.21).
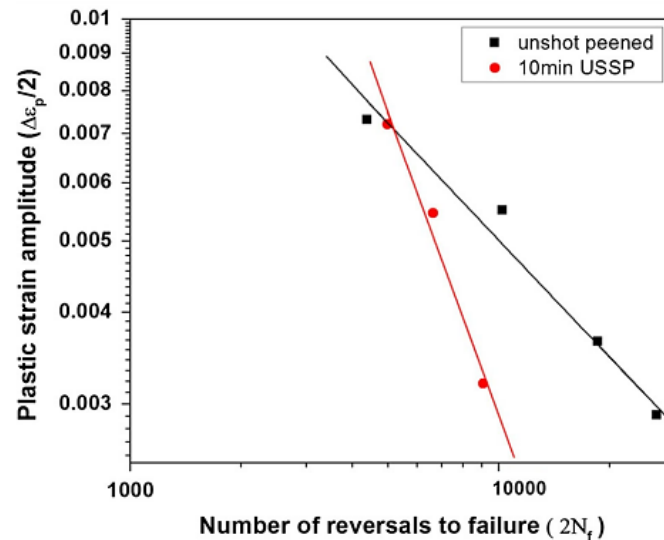
Fig. 1.21 Coffin-Manson plot for non-USSPed and 10 minute USSPed specimens condition [Rai et al. (2014)].

The negative effect of USSP on fatigue life of the USSPed specimen may be attributed to higher surface roughness of the specimen, though, fatigue life is known to improve due to USSP because of associated compressive stresses. However, surface cracks may be generated from USSP for long duration which play negative role on fatigue life. Therefore, the duration of USSP must be proper to control the surface roughness.

1.8 SCOPE OF THE PRESENT INVESTIGATION

As mentioned earlier, there is no systematic study available on the effect of USSP on microstructural modification and electrochemical corrosion. Also no investigation has been reported on hot corrosion of Ti–6Al–4V alloy with surface nanostructure. Also, there is little information on low cycle fatigue behavior of nanostructured Ti–6Al–4V alloy, in particular, at lower strain amplitudes. Therefore, it is worth to carry out a systematic investigation on the effect of USSP on electrochemical corrosion, hot corrosion and LCF of Ti–6Al–4V alloy.

1.9   OBJECTIVES OF THE PRESENT INVESTIGATION

The objectives of the present investigation are listed below:

- Optimization of USSP parameters for surface nanostructuring of the alloy Ti–6Al–4V using hard steel balls of 3 mm diameter.

- Detailed investigation on electrochemical corrosion of ultrasonic shot peened (USSPed) Ti–6Al–4V alloy in synthetic body fluid (Ringer's solution).

- Effect of USSP on hot corrosion behavior of Ti–6Al–4V alloy at 400, 500 and 600 °C.

- Tensile behavior of non-USSPed and USSPed Ti–6Al–4V alloy.

- Systematic investigation on LCF behavior of Ti–6Al–4V alloy in non-USSPed, USSPed and USSPed + stress relieved conditions (400 ℃ for 1h) at room temperature, at different total strain amplitudes and constant strain rate of $5 \times 10^{-3} \text{s}^{-1}$.